PHYSICAL REVIEW B **84**, 060406(R) (2011)

Multiferroicity in $NiBr_2$ with long-wavelength cycloidal spin structure on a triangular lattice

Y. Tokunaga,[1,2] D. Okuyama,[2] T. Kurumaji,[3] T. Arima,[4,5] H. Nakao,[6] Y. Murakami,[6] Y. Taguchi,[2] and Y. Tokura[1,2,3]

[1]*Multiferroics Project, ERATO, Japan Science and Technology Agency (JST), Wako, Saitama 351-0198, Japan*

[2]*Cross-Correlated Materials Research Group (CMRG) and Correlated Electron Research Group (CERG), RIKEN Advanced Science Institute (ASI), Wako, Saitama 351-0198, Japan*

[3]*Department of Applied Physics, University of Tokyo, Bunkyo-ku, Tokyo 113-8656, Japan*

[4]*Department of Advanced Materials Science, University of Tokyo, Kashiwa, Chiba 277-8561, Japan*

[5]*RIKEN SPring-8 Center, Hyogo 679-5148, Japan*

[6]*Condensed Matter Research Center and Photon Factory, Institute of Materials Structure Science, KEK, Tsukuba, 305-0801, Japan*

(Received 25 June 2011; published 26 August 2011)

Multiferroic properties have been investigated for single crystals of the triangular-lattice antiferromagnet $NiBr_2$ with long-wavelength (∼7 nm) cycloidal spin structure whose spin-spiral plane is parallel to (001). X-ray diffraction revealed a magnetoelastic lattice modulation with half the periodicity of the magnetic modulation below the cycloidal ordering temperature ($T_{IC} \sim 23$ K), indicating the elliptically distorted nature of the transverse helix. Field-reversible spontaneous polarization (P) appears in the $[1\bar{1}0]$ direction perpendicular to the spin rotation axis ($\parallel[001]$) below T_{IC}. P shows nontrivial dependence on the magnitude and direction of the poling magnetic field (H), suggesting the possible H selection of the propagation vector of the helix from the sixfold-degenerate directions, even for the in-plane cycloidal spin structure, through magnetic domain control in the higher-temperature spin-collinear antiferromagnetic phase.

DOI: 10.1103/PhysRevB.84.060406 PACS number(s): 75.85.+t, 77.80.Dj, 77.80.Fm, 61.05.cp

Multiferroic materials have recently been studied extensively from the viewpoints of both fundamental physics and possible application to devices.[1,2] In these studies, magnetic and/or electric control of the multiferroic domain is one of the key issues in achieving large magnetoelectric (ME) responses.[3–6] In this context, the spin-spiral magnets (helimagnets) are an important class of multiferroics because their ferroelectric (FE) polarization (P) is induced by the magnetic order, thus producing strong clamping between the FE and magnetic domain walls. In the helimagnetic ferroelectrics, there are two major mechanisms which give rise to the ferroelectricity. One is the spin current or inverse Dzyaloshinskii-Moriya (DM) model,[7–9] which explains P in the transverse spin-spiral (cycloidal) system irrespective of the symmetry of the underlying chemical lattice. According to this model, P is expressed as $P \propto \sum e_{ij} \times (S_i \times S_j)$, where e_{ij} is the unit vector connecting neighboring spins S_i and S_j. Another mechanism is based on the spin-dependent transition-metal–ligand (d-p) hybridization.[10–12] The latter mechanism can also generate P even in the proper-screw system, when the chemical lattice holds some specific symmetry, as in delafossite-type $CuFeO_2$.[13]

In the helimagnetic multiferroics, one way to control the direction of the magnetically induced P with use of a magnetic field (H) is to rotate the spiral plane while keeping the direction of the magnetic modulation vector Q_m unchanged.[14,15] Another way is to change the direction of Q_m itself with use of H, as reported for systems such as cubic $ZnCr_2Se_4$,[5] tetragonal $Ba_2CuGe_2O_7$,[16] and trigonal Ga-doped $CuFeO_2$.[17] In these systems, the high crystal symmetry of the paramagnetic phase allows the existence of domains with different Q_m and P directions (e.g., 60°, 90°, 120°, as well as 180° domains) when the crystal symmetry is lowered by the spiral-spin order. In general, application of H stabilizes the domains with the spiral plane perpendicular to H due to the Zeeman energy gain, thereby leading to a flop of the Q_m and P vectors. In particular, in the case of trigonal Ga-doped $CuFeO_2$,[17] the magnetic structure is proper screw with the (110) spiral plane and the propagation vector along the [110] direction. It is this particular spin structure that allows the magnetic digital flop of P.[17] On the other hand, the mechanism of control of the P domain by H is highly nontrivial when the spin system forms the cycloidal structure which is the other prototypical case of generating P. In this paper, we report on the multiferroic properties as well as H control of P domains in trigonal $NiBr_2$ with long-wavelength cycloidal spin structure by measurements of synchrotron radiation (SR) x-ray diffraction, magnetization (M), and P.

$NiBr_2$ crystallizes in a $CdCl_2$ structure (space group $R\bar{3}m$) as depicted in Fig. 1(a). In this crystal, edge-shared $NiBr_6$ octahedra form two-dimensional triangular lattice sheets, which stack along the [001] direction with weak van der Waals bonding. $S = 1$ spins of Ni^{2+} ions order antiferromagnetically at $T_N = 44$ K. In this collinear antiferromagnetic (AF) phase, the spins on a (001) plane align ferromagnetically, pointing along the $[1\bar{1}0]$ direction [see Fig. 1(c)],[18] while showing the AF stacking along the [001] direction. At $T_{IC} \sim 22.8$ K, a second transition occurs from the collinear to the cycloidal AF phase, in which the spin rotation plane is the (001) plane and the Q_m of the helix is (δ_m δ_m 3/2) with $\delta_m = 0.027$ at 4.2 K, which corresponds to the periodicity of ∼7 nm [Fig. 1(d)].[19–21] As shown in Fig. 1(d) (see also the later discussion), the magnetic point group m' allows P to be perpendicular to the in-plane propagation vector (q_m). Then, six possible directional sets of P and q_m are degenerate in the (001) plane, as depicted in Fig. 1(e).

Single crystals of $NiBr_2$ were grown by the sublimation and Bridgman methods. Thin plates (∼3 × 3 × 0.1 mm^3) with wide faces perpendicular to the crystallographic $[1\bar{1}0]$ and

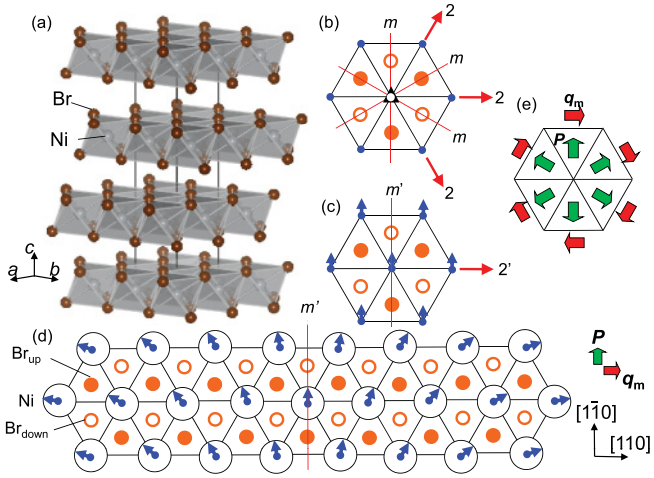

FIG. 1. (Color online) (a) Crystal structure of $NiBr_2$ shown schematically. (b)–(d) Schema of the (b) crystal and (c),(d) magnetic structure and symmetry of $NiBr_2$ in the (001) plane. (c) and (d) depict the collinear layered antiferromagnetic (AF) ($T_{IC} \leqslant T \leqslant T_N$) and cycloidal spin ($T \leqslant T_{IC}$) structures on the triangular lattice, respectively. Small solid arrows indicate spin directions on Ni^{2+} ions. Closed and open small circles represent Br atoms above and below the Ni plane, respectively. (e) Schema of the possible sixfold-degenerate domains with q_m and P vectors. Here, the opposite direction of q_m is defined as spin modulation with opposite helicity.

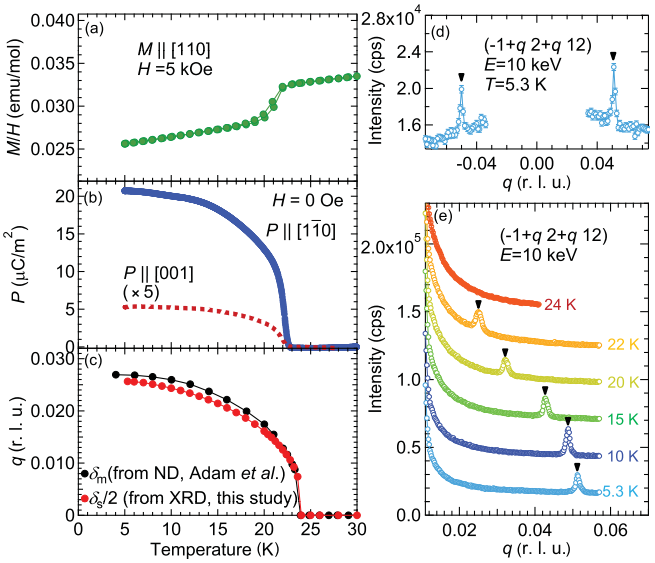

FIG. 2. (Color online) (a)–(c) T dependence of (a) M/H measured at $H = 5$ kOe along the [110] direction, (b) $P \parallel [1\bar{1}0]$ and $P \parallel [001]$ in the absence of H, and (c) $\delta_s/2$ obtained from SR x-ray diffraction measurement (this work) together with the reported δ_m in $Q_m = (\delta_m\ \delta_m\ 3/2)$ [cited from Adam *et al.* (Ref. 19)] from neutron diffraction (ND). (d) X-ray diffraction profile around $(\bar{1}\ 2\ 12)$ measured at 5.3 K. (e) T dependence of $(-1+\delta_s\ 2+\delta_s\ 12)$ superlattice reflection. In (d) and (e), filled triangles indicate the suparlattice peaks.

[001] axes were cut from the single crystal. Electrodes were formed on both sides of the plate with silver paste. P was obtained by integrating the displacement current measured while sweeping temperature (T), H, or electric field (E). Single-crystal x-ray diffraction measurements were made using a four-circle diffractometer on BL-3A at the Photon Factory, KEK, Japan.

As shown in Figs. 2(a) and 2(b), $M \parallel [110]$ shows an anomaly at $T_{IC} \sim 23$ K, below which spontaneous P emerges along the $[1\bar{1}0]$ direction, i.e., perpendicular to the cycloidal spin rotation axis ($\parallel [001]$). While this observation is in accord with the prediction of the inverse DM model,[7–9] the spin-dependent d-p hybridization mechanism[10–12] can also produce an in-plane P component along the same direction, as follows. We observed small but finite $P \parallel [001]$ [$\sim 1\ \mu C/m^2$; see Fig. 2(b)], which is allowed by the symmetry m'. This $P \parallel [001]$ can be explained by the spin-dependent d-p hybridization mechanism,[22] but not by the inverse DM model.[7–9] Assuming that the spin cycloid is of a genuine circle and taking into account the reported value of $\delta_m = 0.027$ at 4.2 K,[19] the calculation based on the d-p hybridization mechanism[10–12] yields $P_{\parallel[001]}/P_{\parallel[1\bar{1}0]} = 0.057$.[22] This is comparable to the experimentally observed value; some ambiguity exists because of the experimental difficulty in the quantitative evaluation of small $P \parallel [001]$. Presumably, both mechanisms may contribute to the observed in-plane P, yet it can be safely said that P resulting from the d-p hybridization mechanism is dominant.

Evolution of the cycloidal spin order was detected by SR x-ray diffraction measurements. Figure 2(d) shows the diffraction profile around $(\bar{1}\ 2\ 12)$ measured at $T = 5.3$ K. Superlattice peaks are observed at $(-1 \pm \delta_s\ 2 \pm \delta_s\ 12)$ with $\delta_s \sim 0.051$. As T is increased, the position of the superlattice peaks monotonically shifts toward the $(\bar{1}\ 2\ 12)$ Bragg peak and finally vanishes at T_{IC} [Fig. 2(e)]. The T dependence of δ_s agrees well with that of twice the reported in-plane magnetic modulation δ_m [see Fig. 2(c)]. The existence of the magnetoelastic lattice modulation with $\delta_s = 2\delta_m$ suggests the elliptically deformed nature of the spin cycloid.[23] (The d-p hybridization mechanism[10] gives rise to $2\delta_m$ charge modulation, which in turn deforms the spin cycloid elliptically also.)

Figures 3(a) and 3(c) show the T dependence of M/H and $P \parallel [1\bar{1}0]$, respectively, measured at various $H \parallel [110]$. As H increases, the FE transition temperature T_c decreases monotonically. A similar monotonic decrease of T_c is also observed when H is applied along $[1\bar{1}0]$, as shown in Fig. 3(b). For these P-T measurements under H, the sample was cooled under E and H from 30 K in the collinear AF phase for the poling, and E was switched off at 5 K prior to the T-increasing run. Interestingly, while the value of $P \parallel [1\bar{1}0]$ at the lowest T (5 K) shows monotonic reduction as $H \parallel [1\bar{1}0]$ is increased, that measured in $H \parallel [110]$ initially increases up to $H = 15$ kOe and then starts to decrease in spite of the same poling E. This means that the FE domains in this system are difficult to align solely by E: While the application of $E \parallel [1\bar{1}0]$ may favor three P domains in which $P \cdot E > 0$ holds, it is difficult to lift the degeneracy among these three [Fig. 3(d)]. Application of $H \parallel [110]$ in addition to E during the poling procedure appears to further lift this degeneracy and tends to align P vector along the E direction [Fig. 3(e)]. Figure 3(f) shows isothermal M-H and P-H curves at 2 K for $H \parallel [110]$. M shows a metamagneticlike first-order transition at around

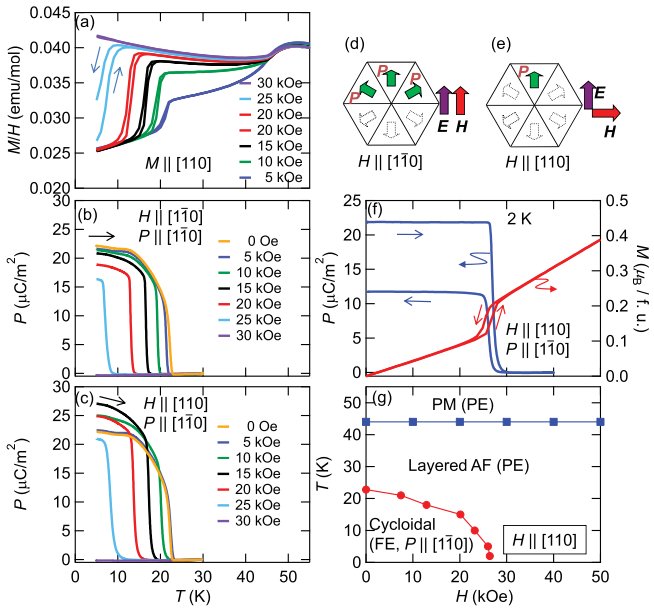

FIG. 3. (Color online) T dependence of (a) $M/H \parallel [110]$ and (b),(c) $P \parallel [1\bar{1}0]$ measured at several H values. Prior to the P-T measurements, the sample was cooled once with the poling field of E and H from the collinear AF phase at 30 K, and then E was removed at 5 K. In (b) and (c), H is applied along $[1\bar{1}0]$ and [110], respectively. (d),(e) Schema of the FE domain population after cooling under $E \parallel [110]$ and H along (d) $[1\bar{1}0]$ and (e) [110], respectively. Short closed (open) arrows indicate P directions of majority (minority) domains. (f) Isothermal P-H and M-H curves measured at 2 K. H is applied along the [110] direction and P along the $[1\bar{1}0]$ direction. (g) ME phase diagram for $H \parallel [110]$ obtained from M and P measurements.

27 kOe, at which P abruptly vanishes. This is ascribed to the transition from cycloidal to collinear AF. P in the H-decreasing run does not fully recover to the initial value. While $P \parallel [001]$ under $H \parallel [110]$ and $H \parallel [1\bar{1}0]$ configurations were also measured (not shown), no enhancement of P was detected, indicating that flop of the spiral plane does not occur, unlike in other cycloidal systems.[14,15,25] In Fig. 3(g) we show the ME phase diagram for $H \parallel [110]$ obtained by measuring M and P. The cycloidal FE phase is not very robust against the application of H parallel to the spiral plane.

Figures 4(a) and 4(b) show the T dependence of $M \parallel [001]$ and $P \parallel [1\bar{1}0]$, respectively, measured at various H along the [001] direction. T_N and T_c are scarcely changed by $H \parallel [001]$, in contrast to the case of $H \parallel [110]$, indicating strong magnetic anisotropy in this compound. These are opposite tendencies to those in Ga-doped $CuFeO_2$ where the spin-spiral plane is the (110) plane.[17] The resultant ME phase diagram for $H \parallel [001]$ is displayed in Fig. 4(c).

In Fig. 5(a), P-E hysteresis loops measured at several temperatures are shown. The opening of the loops observed below T_{IC} clearly shows that P can be directly reversed with E. The coercive force is about 15–20 kV/cm above 10 K, which is larger than that of cycloidal multiferroic $MnWO_4$,[24] but comparable to that of $DyMnO_3$ under $H \parallel b$ of 60 kOe.[25] At 5 K, however, the P-E curve shows no discernible hysteresis loop up to 25 kV/cm, probably because of the reduced mobility

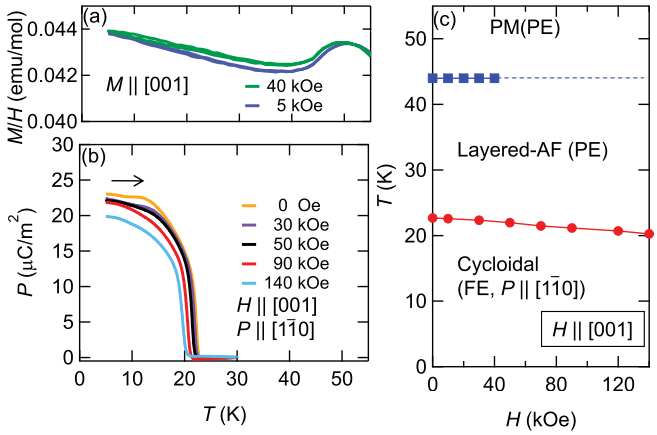

FIG. 4. (Color online) (a),(b) T dependence of (a) $M/H \parallel [001]$ and (b) $P \parallel [1\bar{1}0]$ measured at various H values applied along [001]. Prior to the P-T measurements, the sample was cooled once with the poling field of $E \parallel [1\bar{1}0]$ in the absence of H from the collinear AF phase at 30 K, and then E was removed at 5 K. (c) ME phase diagram with $H \parallel [001]$ obtained from M and P measurements.

of the domain walls of the cycloidal magnetic structure. The remanant P values deduced from the P-E measurements are plotted against T in Fig. 5(c), together with the P value obtained from the pyroelectric current measurement. The data show relatively good agreement above 10 K but exhibit deviation below 10 K. To observe the effect of H during the cooling procedure on the FE cycloidal magnetic domains, we compare P-E hysteresis curves measured at $H = 0$ after zero-field cooling and after field cooling of $H = 20$ kOe in Fig. 5(b). As the sample is cooled in H, the initial curve of the P-E loop tends to be soft, compared with that observed after the zero-field cooling. In addition, a slight increase in the saturation P is observed.

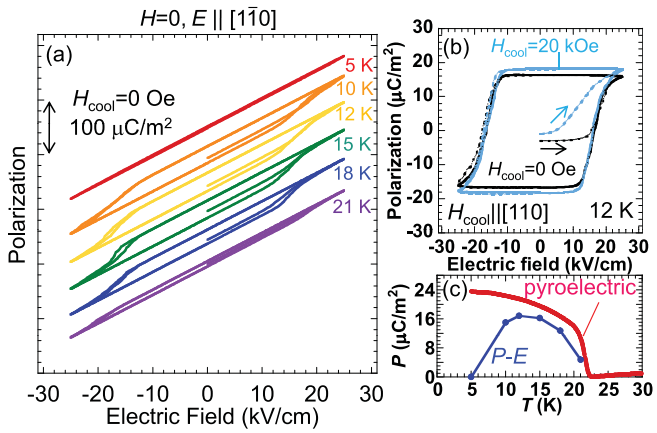

FIG. 5. (Color online) (a) P-E hysteresis loops measured at several temperatures. For clarity, the data are appropriately offset. (b) P-E hysteresis loops measured at $H = 0$ and at 12 K. Black and light blue (gray) curves indicate the data measured after cooling under $H_{cool} = 0$ and 20 kOe, respectively. Dashed and solid lines represent initial and second runs, respectively. The E-linear component of P is subtracted from the raw data. (c) The comparison between P deduced from pyroelectric current measurement and remanant P obtained from P-E hysteresis loops (with E up to 25 kV/cm).

The observed difference in the P-E hysteresis curves as well as the nontrivial dependence of P on the H direction and strength [Figs. 3(b) and 3(c)] suggest that the H during the poling procedure plays an important role in aligning the multiferroic domains. On the other hand, the P cannot be fully controlled by H once the sample is cooled without H. In fact, the isothermal P-H curve [Fig. 3(f)] shows an almost constant P value as H is increased until the cycloidal order is destroyed, suggesting that no flop of the spiral plane or q_m vector occurs. These facts can be accounted for in terms of the cycloidal spin structure and its emergence from the collinear layered AF structure. Because the spiral plane is parallel to the (001) plane, there is little difference in the stability of the domains with $q_m \parallel \langle 110\rangle$ between the field directions of $H \parallel [110]$ and $H \parallel [1\bar{1}0]$, thereby resulting in no flop of the q_m vector. Nevertheless, H can affect the spin structure in the collinear AF phase with significant in-plane anisotropy. The direction of the sublattice spins in the collinear AF phase is along the $\langle 1\bar{1}0\rangle$ axis in the present setting.[18] As depicted in Fig. 1(c), in this collinear AF phase, the magnetic point group is $2'/m'$, which is already monoclinically deformed from the parent structure (point group $\bar{3}m$); namely, two mirrors and two twofold rotation axes have already been lost due to the magnetostriction. Upon the further transition to the cycloidal state at T_{IC}, the twofold rotation axis ($2'$) is further lost and only one mirror plane (m') survives, with q_m running perpendicular to it. Therefore, the direction of the sublattice spins of the high-T collinear AF phase determines the direction of q_m in the low-T cycloidal phase. In the collinear AF phase, application of $H \parallel [110]$ stabilizes the particular AF domains in which sublattice spins are directed along the $[1\bar{1}0]$ axis. Because the creation of the new mirror plane along a different direction needs additional energy, only $q_m \parallel [110]$ domains with $P \parallel [1\bar{1}0]$ are populated in the cycloidal phase via the field-cooling procedure by way of the collinear AF state. Such a field-cooling effect also explains the increase of residual P in the P-E hysteresis loops.

In conclusion, we have revealed multiferroic properties for single crystals of the triangular-lattice antiferromagnet $NiBr_2$ with cycloidal spin structure. An x-ray diffraction study has unraveled the elliptically deformed nature of the transverse helix. The T dependence of M and P indicates that a field-reversible spontaneous P appears in the $[1\bar{1}0]$ direction below $T_{IC} \sim 23$ K. The observed P shows nonmonotonic dependence on the magnitude and direction of the poling H, suggesting the selection of a unique cycloidal q_m vector from the sixfold-degenerated directions by means of H.

This work was in part supported by Grant-in-Aids for Scientific Research from the MEXT, Japan and the Funding Program for World Leading Innovative R&D on Science and Technology (FIRST) on "Quantum Science on Strong Correlation."

[1] S.-W. Cheong and M. Mostovoy, Nature Mater. **6**, 13 (2007).
[2] Y. Tokura and S. Seki, Adv. Mater. **22**, 1554 (2010).
[3] Y. Yamasaki, S. Miyasaka, Y. Kaneko, J.-P. He, T. Arima, and Y. Tokura, Phys. Rev. Lett. **96**, 207204 (2006).
[4] F. Kagawa, M. Mochizuki, Y. Onose, H. Murakawa, Y. Kaneko, N. Furukawa, and Y. Tokura, Phys. Rev. Lett. **102**, 057604 (2009).
[5] H. Murakawa, Y. Onose, K. Ohgushi, S. Ishiwata, and Y. Tokura, J. Phys. Soc. Jpn. **77**, 043709 (2008).
[6] A. Scaramucci, T. A. Kaplan, and M. Mostovoy, e-print arXiv:0906.5298.
[7] H. Katsura, N. Nagaosa, and A. V. Balatsky, Phys. Rev. Lett. **95**, 057205 (2005).
[8] M. Mostovoy, Phys. Rev. Lett. **96**, 067601 (2006).
[9] I. A. Sergienko and E. Dagotto, Phys. Rev. B **73**, 094434 (2006).
[10] T. Arima, J. Phys. Soc. Jpn. **76**, 073702 (2007).
[11] C. Jia, S. Onoda, N. Nagaosa, and J. H. Han, Phys. Rev. B **74**, 224444 (2006).
[12] C. Jia, S. Onoda, N. Nagaosa, and J. H. Han, Phys. Rev. B **76**, 144424 (2007).
[13] T. Kimura, J. C. Lashley, and A. P. Ramirez, Phys. Rev. B **73**, 220401(R) (2006).
[14] T. Kimura, T. Goto, H. Shintani, K. Ishizaka, T. Arima, and Y. Tokura, Nature (London) **426**, 55 (2003).
[15] K. Taniguchi, N. Abe, T. Takenobu, Y. Iwasa, and T. Arima, Phys. Rev. Lett. **97**, 097203 (2006).
[16] H. Murakawa, Y. Onose, and Y. Tokura, Phys. Rev. Lett. **103**, 147201 (2009).
[17] S. Seki, H. Murakawa, Y. Onose, and Y. Tokura, Phys. Rev. Lett. **103**, 237601 (2009).
[18] R. J. Pollard, V. H. McCann, and J. B. Ward, J. Phys. C **15**, 6807 (1982).
[19] A. Adam, D. Billerey, C. Terrier, R. Mainard, L. P. Regnault, J. Rossat-Mignod, and P. Mériel, Solid State Commun. **35**, 1 (1980).
[20] P. Day, A. Dinsdale, E. R. Krausz, and D. J. Robbins, J. Phys. C **9**, 2482 (1976).
[21] P. Day and K. R. A. Ziebeck, J. Phys. C **13**, L523 (1980).
[22] T. Kurumaji *et al.* (unpublished).
[23] T. Arima, Y. Yamasaki, T. Goto, S. Iguchi, K. Ohgushi, S. Miyasaka, and Y. Tokura, J. Phys. Soc. Jpn. **76**, 023602 (2007).
[24] B. Kundys, C. Simon, and C. Martin, Phys. Rev. B **77**, 172402 (2008).
[25] T. Kimura, G. Lawes, T. Goto, Y. Tokura, and A. P. Ramirez, Phys. Rev. B **71**, 224425 (2005).